

# WTKO-CNN: Deep Learning Reveals Sequence Motifs Distinguishing Wild-Type and Knockout ATAC-seq Peaks

Lopamudra Dey

May 26, 2026

## 1 Abstract

Chromatin regulators can alter transcriptional programs by modifying the accessibility of regulatory DNA elements. Understanding how regulatory sequences differ between wild-type (WT) and knockout (KO) conditions is crucial for deciphering transcriptional control. Here, we applied a convolutional neural network, **WTKO-CNN** with an attention mechanism to classify DNA sequences as WT or KO, achieving high predictive performance. To interpret the model, we generated saliency maps to identify nucleotide positions most influential for the classification decision. From these high-saliency regions, we extracted and clustered k-mers, enabling de novo motif discovery. Sequence logos and consensus motifs derived from the CNN filters revealed biologically meaningful patterns, which are further validated using MEME, TOMTOM, and HOMER against known transcription factor binding sites. Our analysis identified motifs associated with transcription factor families that discriminate WT from KO sequences, demonstrating that CNN-guided saliency mapping is a powerful approach for uncovering functional sequence features.

## 2 Introduction

The Transposase Accessible Chromatin Assay (ATAC-seq) data is the most recent significant method to assess genome-wide chromatin accessibility accurately. Over the years, both determining areas that are differentially accessible (DA) between two cellular states and identifying basal accessible chromatin regions within a specific cellular context have been accomplished using ATAC-seq [16]. Transcription factors (TF), which bind to particular DNA sequences to modify transcriptional activity, are crucial for the control of genes [3]. Understanding the relationship between transcription factor (TF) binding and chromatin accessibility is essential for understanding transcriptional regulation, cell state control, and the emergence of novel phenotypes. TFs can identify their motifs and control gene expression programs in putatively open regions that have been cataloged by recent genome-wide chromatin accessibility profiling studies [17, 12, 20].

Deep learning models have been increasingly popular in recent years and have produced ground-breaking findings in a wide range of scientific fields [14, 4, 18, 5]. Due to the intricate architecture, these deep learning models are frequently referred to as "black boxes" despite their excellent predictive ability. This "black box" style makes it challenging to understand how predictions are made. However, model interpretability is critical in biological research since prediction accuracy is just as important as comprehending the underlying sequence characteristics and regulatory logic controlling gene expression. To open this black box, we propose **WTKO-CNN**, a two-layer convolutional neural network with saliency map that exploits k-mer representations derived from ATAC-seq data to reveal sequence determinants underlying differences between wild-type (WT) and knockout (KO) chromatin accessibility regions. By facilitating the direct extraction of informative k-mer patterns, WTKO-CNN prioritises interpretability over traditional deep learning approaches. The learned convolutional filters correspond to sequence motifs that provide mechanistic insight into regulatory alterations induced by gene knockout.

Recently, deep learning approaches, particularly convolutional neural networks (CNNs) have been applied to genomic sequences, enabling automated feature extraction and the identification of sequence regions most predictive of TF binding through saliency maps [23]. These methods are used in many researches

for better peak-detection and classification compared to traditional peak-calling tools such as MACS2 [7, 14]. In many research works, it can be seen that combining CNN and LSTM in a hybrid model is a powerful approach for DNA sequence classification tasks [18, 5]. In [24], the authors suggested deep learning techniques such as CNN, DNN, and the N-gram probabilistic model to classify DNA sequences. Based on the distance measure, a novel method for feature extraction using the random DNA sequence is put forth. The CNN layers are responsible for extracting local sequence features, such as short k-mers or motifs, by applying convolutional filters to the one-hot encoded DNA sequences. These local patterns are then downsampled using pooling layers to reduce dimensionality [15]. In [26] the authors introduced DeepSEA, a deep convolutional neural network capable of predicting chromatin effects directly from DNA sequence. The model demonstrated that deep learning can automatically learn regulatory sequence features without manual feature engineering. Later, interpretability became an important research direction. In [9], an interpretability model is provided by the Deep Motif Dashboard (DeMo Dashboard), which aims to clarify how deep neural networks categorise transcription factor binding sites (TFBS). They evaluated three methods, convolutional (CNN), recurrent (RNN), and hybrid CNN-RNN architectures and using saliency maps, they identifies high-contribution nucleotides via first-order derivatives, and temporal output scores. Zhang et al. proposed a new architecture CAE-CNN (Convolutional AutoEncoder and Convolutional Neural Network) by combining a convolutional autoencoder with convolutional neural network. They used a highway connection layer to capture DNA nucleotide patterns, and extensive evaluations on human and mouse TFBS datasets and demonstrates that an integrated unsupervised-supervised approach outperforms state-of-the-art methods in motif discovery with accuracy, precision, recall, and AUC [25]. In [8], the authors showed that motif extraction from deep CNNs is difficult due to its scattered representations and also improved test performance does not ensure interpretability. They tested CNN on synthetic and actual DNA sequences and demonstrates that adding exponential activations to first-layer filters results in more robust and interpretable motif representations. DeepSite uses CNN and bidirectional long short-term memory to identify long-term relationships between DNA sequence motifs. Apart from taking sequence dependencies into account, they found how to get motif information in the imbalanced data and filter out legitimate information in huge data [19]. To maximise motif prediction, Yang et al. used binomial distribution and deep neural networks in [21]. There are certain issues with prediction accuracy and runtime performance, despite the fact that current deep learning techniques have produced good results in TFBS discovery. In [10] the authors provide a novel two-step model called the Salient Relevance (SR) map, which attempts to clarify how deep CNNs identify images and extract characteristics from regions known as attention areas. Another work, **DeepLIFT** (Deep Learning Important Features) decomposed the contributions of individual nucleotides within one-hot encoded sequences to the final model output. The model explains neural network predictions by tracing how differences from a baseline input propagate through the network and assigning importance scores to each input feature [11]. To improve transparency, [13] proposed ExplaiNN, an interpretable neural network architecture for genomics. ExplaiNN consists of multiple independent convolutional units, where each unit learns a motif-like feature from DNA sequences. These features are combined through a linear layer, allowing researchers to easily interpret the contribution of each learned motif to the final prediction. Other model explanation techniques, such as SHAP and Integrated Gradients, have also been widely used to interpret neural network predictions in genomics. These approaches help identify biologically meaningful sequence motifs and regulatory patterns. Overall, recent research focuses on building models that not only achieve high predictive performance but also provide biological interpretability.

Recurrent neural networks (RNNs) are capable of modelling DNA sequences, however they often provide limited interpretability and are less successful at discovering brief, position-independent motifs. Convolutional neural networks, on the other hand, are more appropriate for interpretable assessments of variable chromatin accessibility because they directly capture k-mer-like patterns that correlate to transcription factor binding sites. In order to prioritize interpretability, we chose a CNN-only strategy even though hybrid CNN-LSTM structures can reflect higher-order dependencies between sequence motifs. Convolutional filters effectively capture the presence or lack of transcription factor binding motifs, which are the main cause of changes in chromatin accessibility between wild-type and knockout circumstances. The proposed WTKO-CNN model achieved a training accuracy of around 92% and a test accuracy of approximately 68% with RelA WT and KO Peaks. Saliency map analysis helps to identify discriminating kmers. These k-mers are clustered using agglomerative clustering to generate consensus motifs, enabling the identification of discriminative sequences. This analysis demonstrates that chromatin accessibility differences are largely driven by

transcription factor binding, and that recurrent layers increase model complexity without providing clear gains in motif interpretability, reinforcing our decision to use a CNN-only architecture. Despite advances in CNN-based motif discovery, relatively few studies integrate saliency-driven k-mer extraction with clustering to systematically compare WT and KO sequences, highlighting the need for approaches that can robustly identify discriminative motifs between conditions. Our study leverages this combined workflow to uncover TF motifs that differentiate WT from KO, providing insight into the regulatory logic underlying the observed genomic differences. WTKO-CNN scripts along with all commands are available from the GitHub repository (<https://github.com/LopamudraDey/WTKO-CNN>). We used `cnn_attention` for model training and classification, `test_attention` for evaluating WT vs KO sequences, and `motif_attention` for extracting high-saliency k-mers and performing motif analysis.

### 3 Materials and Methods

#### 3.1 Dataset

We evaluated the performance of our convolutional neural network (CNN) using two distinct biological paradigms of transcriptional and epigenetic regulation. These datasets are retrieved from the Gene Expression Omnibus (GEO) and consist of differentially accessible regions (ATAC-seq) comparing Wild-Type (WT) and Knockout (KO) genotypes in *Mus musculus*.

- **GSE107075 (RelA):** ATAC-seq data for the RelA knockout (KO) and wild-type (WT) mouse fibroblasts are obtained from the Gene Expression Omnibus (GEO) under accession GSE107075 [2] (<https://www.ncbi.nlm.nih.gov/gds/?term=GSE107075>). The dataset was generated using the Illumina NextSeq 500 platform and contains chromatin accessibility profiles from mouse fibroblasts under WT and KO conditions with two biological replicates each. The experiment aimed to identify genomic regions exhibiting differential chromatin accessibility following deletion of the transcription factor RelA, a key component of the complex.
- **GSE119222 (LSD1):** ATAC-seq data, containing chromatin accessibility profiles from germinal center B cells in *Mus musculus*, including two WT and three LSD1 knockout samples, generated from sorted GC B splenocytes ten days after immunization (<https://www.ncbi.nlm.nih.gov/geo/query/acc.cgi?acc=GSE119222>) [6].

The final distribution of genomic sequences utilized for model training and validation of these two datasets is added in Table 1 with GEO ID, number of WT and KO samples with target factor.

Table 1: Summary of Experimental Datasets and Sample Sizes

GEO ID	Target Factor	WT ( $n$ )	KO ( $n$ )	Total ( $N$ )
GSE107075	RelA (p65)	3722	6164	9886
GSE119222	LSD1	315	733	1,048

#### 3.2 CNN-Based Peak Prediction and Discriminative K-mer Extraction

To investigate whether DNA sequence features alone can distinguish between Ebf1 WT and KO chromatin accessibility, we developed a convolutional neural network (WTKO-CNN) model for binary peak classification. An overview of the CNN-based WT and KO ATAC-seq peak classification pipeline is provided in Figure 1, illustrating the sequential steps from peak preprocessing and one-hot encoding to dataset balancing, model training, and performance evaluation.

##### 3.2.1 Data Preprocessing: Extraction and Labeling of Sequences

To prepare genomic data for convolutional neural network (CNN) analysis, raw ATAC-seq peaks are processed to ensure uniform input dimensions. For each differentially accessible region, the summit of the peak defined

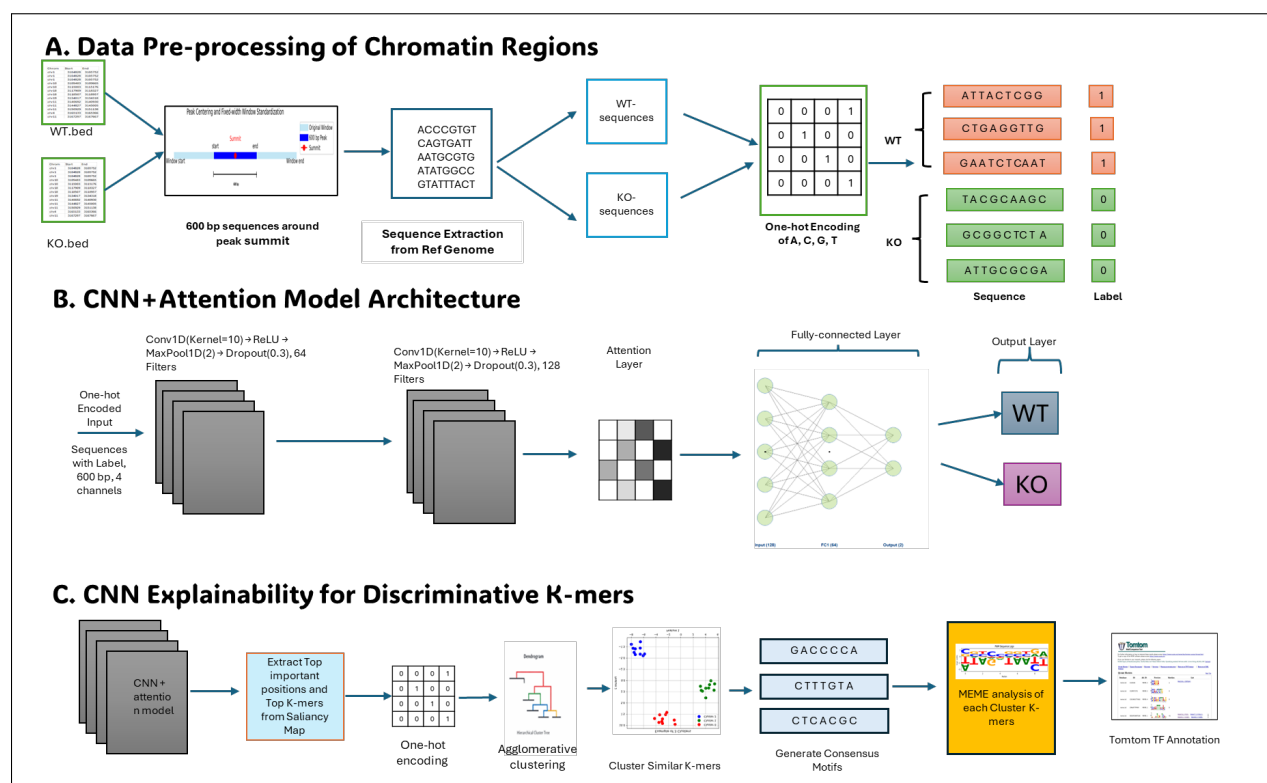


Figure 1: Schematic overview of the CNN-based pipeline for WT and KO ATAC-seq peak classification. (A) Data preprocessing steps, including sequence extraction of peaks from reference genome, one-hot encoding of DNA sequences, and class labelling of WT- and KO-specific peaks. (B) Convolutional neural network architecture for supervised classification of WT- and KO-specific ATAC-seq peaks based on sequence features for peak prediction. (C) Saliency-guided k-mer extraction and motif analysis. Saliency maps derived from the trained CNN are used to identify the most informative nucleotide positions within each sequence. Twenty-base-pair k-mers centered on high-saliency positions are extracted and subsequently clustered using agglomerative clustering to group similar sequence patterns. Consensus motifs are generated from each cluster using MEME, and the resulting motifs are compared against known transcription factor databases using TOMTOM to identify candidate regulatory factors associated with condition-specific chromatin accessibility.

as the genomic coordinate with the maximum read density was identified. Then a fixed-width regulatory window of 600 bp was defined by centring on the summit (summit  $\pm$  300 bp). This centering strategy ensures that core regulatory features, including transcription factor binding sites (TFBS), which tend to cluster near peak summits, are consistently positioned within the receptive field of the first convolutional layer. Both these RelA and LSD1 datasets are available in Supplementary File S1. The resulting genomic windows are

Position	Base	Encoding
1	A	[1, 0, 0, 0]
2	C	[0, 1, 0, 0]
3	G	[0, 0, 1, 0]
4	T	[0, 0, 0, 1]
5	N	[0, 0, 0, 0]

Table 2: One-hot encoding of the nucleotide sequence “ACCCGTCA”

extracted from the mm10 reference genome, yielding sequences of uniform length (600 bp). Each sequence was encoded using a one-hot representation with four channels corresponding to the nucleotides A, C, G, and T. Specifically, adenine (A) was encoded as [1, 0, 0, 0], cytosine (C) as [0, 1, 0, 0], guanine (G) as [0, 0, 1, 0], and thymine (T) as [0, 0, 0, 1]. Ambiguous nucleotides (N) are represented as [0, 0, 0, 0] (Table 2). An example of one-hot encoding for the sequence “ACCCGTCA” is shown in Figure 2. The

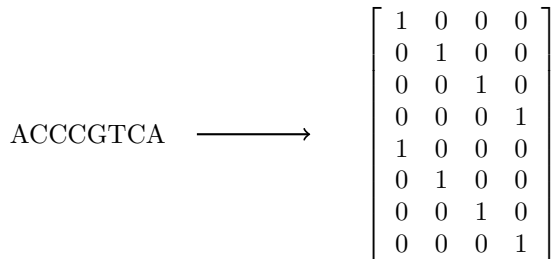


Figure 2: Illustration of sequence ”ACCCGTCA” being transformed into a one-hot encoded matrix and fed into a CNN layer for further processing.

one-hot encoded sequence is treated by the CNN as a two-dimensional input matrix (e.g.,  $8 \times 4$  for the illustrative example), where rows correspond to nucleotide positions and columns correspond to nucleotide identities. Convolutional filters (kernels) scan this matrix to learn local sequence patterns and regulatory motifs relevant to chromatin accessibility.

As the downstream task involved binary peak classification, each sequence was assigned a class label based on condition-specific chromatin accessibility. Peaks specific to the wild-type (WT) condition are assigned label 1, whereas peaks specific to the knockout (KO) condition are assigned label 0. The one-hot encoded sequences and their corresponding labels are used as inputs for training the convolutional neural network (CNN) model. To avoid bias during training, class imbalance between WT- and KO-specific peaks was corrected by balancing the dataset according to peak counts, resulting in an equal number of sequences for each class used in supervised learning.

The CNN architecture was designed with two convolutional layers to hierarchically extract regulatory sequence features from the one-hot encoded DNA inputs. Because peak lengths varied substantially across the dataset (ranging from 150 to 2567 bp), all sequences are standardized to a fixed length of 600 bp prior to training. This length was empirically determined using saliency map analysis, which indicated that the most informative and discriminative sequence features are typically concentrated within an approximately 600 bp window centered on the peak summit. Standardizing sequence length ensured consistent input dimensions for the CNN while preserving the most biologically relevant signal.

The convolutionally generated feature maps are subjected to an attention layer to further identify physiologically significant regions within each sequence. In order to create attention weights that indicate the relative significance of each position in the sequence, an attention score was calculated for each position and

normalised using the softmax algorithm. The model was able to concentrate on the most informative areas for classification since the final sequence representation was produced as a weighted sum of positional feature vectors.

### 3.2.2 Training and Test Split

Following sequence preprocessing, one-hot encoding, and dataset balancing, we implemented a supervised convolutional neural network (CNN) to classify ATAC-seq peaks as WT- or KO-specific based solely on their underlying DNA sequence. To prevent data leakage, sequences from chromosomes 6 and 7 are held out as a test set, while sequences from the remaining chromosomes are used for training. This ensured that the model was evaluated on completely independent, unseen genomic regions, which is essential for a fair and realistic assessment of model performance and further use of the model for peak prediction for other unseen regions.

### 3.2.3 CNN Architecture

Each input sequence was represented as a  $600 \times 4$  matrix, where rows corresponded to nucleotide positions and columns to nucleotides (A, C, G, T). The CNN architecture consisted of two one-dimensional convolutional layers. The first layer contained 64 filters with a kernel size of 10 bp, followed by batch normalization, ReLU activation, max-pooling, and dropout (rate = 0.3). The second convolutional layer contained 128 filters (kernel size = 10 bp), with similar batch normalization, ReLU, max-pooling, and dropout. This design allows the network to learn motif-like sequence features while reducing overfitting.

The output of the convolutional layers was flattened and passed through a fully connected layer of 64 neurons, followed by a two-node output layer with a softmax activation to predict WT or KO class probabilities. The model was trained using the Adam optimizer with an initial learning rate of 0.001, L2 weight decay (0.0001), and binary cross-entropy loss. Mixed precision training and gradient accumulation (steps = 4) are used to improve efficiency and stability. Training was performed for 100 epochs, with the best model selected based on maximum test set accuracy. Training was performed in mini-batches of sequences for up to 100 epochs (Table 3).

### 3.2.4 Model Training

The model was implemented in PyTorch and trained using the Adam optimizer with a learning rate of  $3 \times 10^{-4}$  and weight decay of  $1 \times 10^{-4}$ . Cross-entropy loss was used as the optimization objective. Training was performed for 100 epochs with gradient accumulation to simulate larger batch sizes. Mixed-precision training was enabled when GPU hardware was available.

### 3.2.5 Model Evaluation

After training, the best-performing model was used to predict labels for the test set. Performance was assessed using overall accuracy, confusion matrix, and classification metrics including precision, recall, and F1-score for each class. Model performance was monitored per epoch, tracking both training and test accuracy. This pipeline enabled identification of sequence features predictive of chromatin accessibility differences between WT and KO conditions. The best model checkpoint was saved for downstream evaluation. The CNN architecture used in this study is summarized in the following pseudocode. The model integrates convolutional feature extraction with an attention mechanism for sequence-level classification.

Listing 1: Pseudocode for CNN-based Chromatin Accessibility Classification

```
Input: WT and KO DNA sequences (variable length, padded to 600 bp)
Labels: WT = 1, KO = 0

\begin{lstlisting}[caption=CNN + Attention Model for Chromatin Accessibility
Classification]
```

Input: WT/KO DNA sequences (padded to 600 bp), labels (WT=1, KO=0)

1. Data:

- Balance WT and KO samples
- Split by chromosome:
  - Train: chromosomes 1-19 Except Chromosome 6 and 7
  - Test: chromosome 6 and 7
- One-hot encode (A,C,G,T,N) (600 4)

2. Model:

- Input reshape to (batch, 4, 600)
- Conv1D(64, kernel=10) + ReLU + MaxPool + Dropout(0.3)
- Conv1D(128, kernel=10) + ReLU + MaxPool + Dropout(0.3)
- Attention over sequence dimension
- Dense(128->64) + ReLU
- Dense(64->2 logits)

3. Training:

- Loss: CrossEntropyLoss
- Optimizer: Adam (lr=0.001)
- Mixed precision (autocast + GradScaler)
- Gradient accumulation (4 steps)
- Train for 100 epochs

4. Evaluation:

- Test on chr6/chr7 each epoch
- Save best model by test accuracy
- Final metrics: confusion matrix, precision, recall, F1

5. Output:

- Accuracy curves
- Confusion matrix
- Best model weights

6. Interpretation:

- Saliency maps

Table 3: Architecture of the 1D Convolutional Neural Network with Attention for sequence classification.

Layer	Type	Parameters	Activation
Input	Sequence	600 × 4 nucleotides	—
Conv1D (1)	Convolutional	64 filters, kernel size=10	ReLU
Max Pool (1)	Max Pooling	pool size=2	—
Dropout (1)	Regularization	$p = 0.3$	—
Conv1D (2)	Convolutional	128 filters, kernel size=10	ReLU
Max Pool (2)	Max Pooling	pool size=2	—
Dropout (2)	Regularization	$p = 0.3$	—
Attention	Attention	128-dimensional feature vectors	Softmax weights
Fully Connected	Linear	64 units	ReLU
Output	Linear	2 units (Logits)	—

### 3.3 Saliency-Based Identification of Regulatory Sequence Features

To interpret the regulatory sequence patterns learned by the WTKO-CNN model, we applied gradient-based attribution using saliency mapping to estimate the contribution of individual nucleotide positions to the model’s predictions. For a given input sequence  $X \in \{0, 1\}^{L \times 4}$ , where  $L = 600$ , the saliency map  $S(X)$  was defined as the gradient of the predicted class logit  $f_c(X)$  (pre-softmax) with respect to the input sequence:

$$S(X) = \frac{\partial f_c(X)}{\partial X} \tag{1}$$

The magnitude of this gradient reflects the local sensitivity of the models prediction to perturbations at each nucleotide position. Because DNA sequences are represented using one-hot encoding, gradients are computed across the four nucleotide channels  $j \in \{A, C, G, T\}$ . To obtain a single positional importance score  $M_i$ , we selected the maximum absolute gradient value across the nucleotide channels:

$$M_i = \max_{j \in \{A, C, G, T\}} |S_{i,j}| \tag{2}$$

This operation produced a position-wise importance profile for each sequence, where nucleotides with the highest saliency scores are interpreted as the most influential features contributing to the classification decision.

For each sequence in the test dataset (chromosomes 6 and 7), the three positions with the highest  $M_i$  values are identified as saliency peaks. Positions with the highest saliency scores are interpreted as the most influential regions contributing to the classification decision. For each sequence in the test dataset, the top three highest-scoring positions are identified. To capture potential regulatory motifs, 20-bp  $k$ -mers centered on each peak position  $p_n$ , centered around these high-importance positions are extracted.

$$k\text{-mer}_n = X[p_n - 6 : p_n + 7] \tag{3}$$

The potential regulatory motifs that underlie the differences in accessibility between WT and KO situations are represented by these extracted subsequences. For further analysis and visualisation, these motif candidates are gathered. Saliency maps are also created for each sequence to show how positional importance is distributed across the sequence and to emphasise the areas that have the biggest impact on the model’s predictions.

### 3.4 Motif Discovery from Saliency-Identified k-mers

To identify the sequence motifs learned by the WTKO-CNN model, top  $k$ -mers (20bp) centered on saliency peaks are first extracted from each sequence. Each sequence contributed multiple  $k$ -mers corresponding to its highest-saliency positions. These  $k$ -mers are then flattened into a single table, with each row representing one  $k$ -mer and its associated sequence index and position.

The flattened  $k$ -mers are numerically encoded using one-hot representation for the four standard nucleotides (A, C, G, T), with ambiguous positions treated as a separate channel. Next, these  $k$ -mers are clustered using agglomerative hierarchical clustering. We used cosine distance and average linkage, to group similar sequence patterns into clusters. For each cluster, a consensus motif and a weighted position matrix are computed. Then MEME is applied on each cluster  $k$ -mer fasta sequences separately.

The motifs identified by MEME are compared with known transcription factor binding site (TFBS) databases using TOMTOM, allowing us to associate CNN-derived sequence features with established regulatory elements. This workflow enabled systematic interpretation of the sequence features driving model predictions and facilitated direct comparison with known TFBS. Figure 3 illustrates the workflow for saliency-based motif discovery from the WTKO-CNN model.

### 3.5 Identification of Discriminative $k$ -mers

Importantly, in this work, we applied explainable AI (XAI) methods to learn more about how our CNN model makes decisions. To ensure the model learned generalizable biological motifs rather than locus-specific features, we implemented a strict genomic partition. Filters are optimized using sequences from the majority

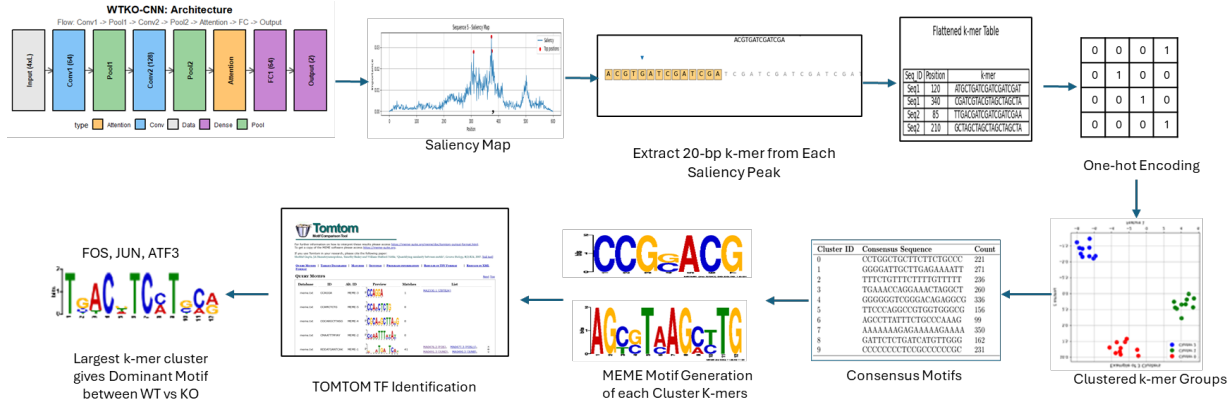


Figure 3: The workflow for motif discovery from the WTKO-CNN model, including saliency-based k-mer extraction, clustering, motif generation, and comparison with known TFBS using MEME and TOMTOM.

of the genome, while Chromosomes 6 and 7 are held out as an independent test set. This spatial separation ensures that the motifs identified by our convolutional filters represent conserved regulatory signatures across the entire murine genome. We extracted attention-weighted k-mers from the model to identify candidate regulatory elements enriched in either WT or KO peaks. This method not only helped us identify the sequence elements that are essential to the model’s predictions, but it also made it possible to link these significant regions to motifs that had biological significance. We found k-mers that are aggregated from saliency scores using a sliding window approach, and ranked them according to how relevant they are to the classification job.

To identify sequence motifs associated with WT- and KO-specific chromatin accessibility, we extracted k-mers from the first convolutional layer of our trained CNN models. We analyzed the weights of the first convolutional layer. Each of the 64 filters represents a position weight matrix (PWM) of length  $k = 10$ . We converted these weights into consensus k-mers by identifying the nucleotide with the maximum weight at each position:

$$S_j = \operatorname{argmax}_{i \in \{A, C, G, T\}} W_{i,j} \quad (4)$$

where  $W_{i,j}$  represents the weight of nucleotide  $i$  at position  $j$ . Given that random weight initialization and dropout can result in slight variability in learned filters, we trained the network independently five times, each with a unique random seed. For each run, high-activation subsequences corresponding to the convolutional filters are collected as candidate k-mers.

To ensure robust motif identification, we aggregated k-mers across all five runs and retained only those that are consistently detected in multiple models, thereby emphasizing recurrent and biologically relevant patterns. Extracted k-mers are subsequently analyzed using motif discovery tools, allowing comparison with known transcription factor binding sites and identification of novel regulatory elements underlying differential chromatin accessibility between WT and KO conditions.

The model was shown to have learned biologically important patterns when the top-ranked k-mers are compared with known transcription factor binding motifs from JASPAR and HOMER. The interpretability of our CNN model is further demonstrated by the identification of unique motifs that are absent from both databases, indicating the approach’s potential to find new regulatory components. In addition to validating the model’s predictions, this combination of XAI approaches bridges the gap between machine learning and biological knowledge by offering a deeper understanding of the chromatin accessibility landscape. The figure 4 shows the Interpretability Pipeline for Genomic Sequence Classification.

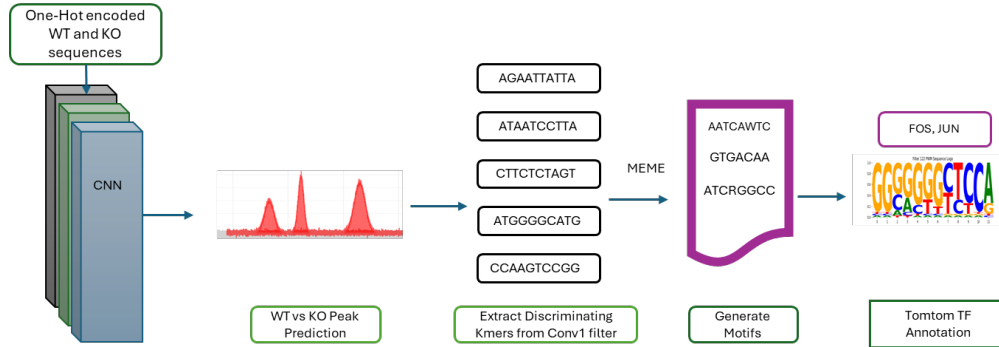


Figure 4: **Schematic of the Interpretability Pipeline for Genomic Sequence Classification.** One-hot encoded Wild Type (WT) and Knockout (KO) sequences are fed into a deep learning model to classify the peak. To interpret the model, discriminating k-mers are extracted from the learned filters. These sequences are processed using MEME [1] for motif discovery, and the resulting motifs are annotated with transcription factor (TF) identities using Tomtom.

## 4 Results

### 4.1 Model Training and Performance

To evaluate the ability of WTKO-CNN to capture sequence determinants of chromatin accessibility, we trained the model on genome-wide ATAC-seq data while holding out chromosomes 6 and 7 for independent testing. This chromosome-level holdout ensures that performance reflects the models ability to generalize to unseen genomic regions, rather than memorizing training sequences. On the held-out chromosomes, WTKO-CNN accurately distinguished wild-type (WT) from knockout (KO) peaks, achieving, demonstrating robust predictive performance across the genome. The CNN was trained to classify WT- and KO-specific ATAC-seq peaks based on 600 bp one-hot encoded sequences. Training was performed for 100 epochs with gradient accumulation and mixed precision. Early epochs showed a steady increase in both training and test accuracy. Beyond this point, the training accuracy continued to increase, while test accuracy decreases, indicating overfitting .

Due to stochastic weight initialization and data shuffling, model performance can vary slightly across runs. To ensure robustness, we trained the model multiple times and reported the best-performing model results. WTKO-CNN was evaluated on two independent ATAC-seq datasets (GSE107075, GSE119222) to assess its generalization beyond the training data. As shown in Table 4, the model achieved moderate to high accuracy, ranging from 68% to 84%, with per class precision, recall, and F1-scores reflecting variability between wild-type (WT) and knockout (KO) peaks. Figure 5 shows the confusion matrix of the WTKO-CNN prediction. Differences in performance across datasets likely arise from a combination of factors, including technical variations in ATAC-seq protocols, biological heterogeneity of the samples, and subtle differences in the magnitude of chromatin accessibility changes between WT and KO conditions. Despite these variations, WTKO-CNN consistently identified informative k-mer patterns corresponding to transcription factor binding motifs enriched in condition-specific peaks, demonstrating its ability to capture biologically meaningful regulatory features even in external datasets.

Table 4: Performance of WTKO-CNN on held-out chromosomes and training data.

Dataset	Class	Precision	Recall	F1-score	Accuracy
GSE107075	WT	0.73	0.57	0.64	68%
	KO	0.65	0.79	0.71	
GSE119222	WT	0.83	0.87	0.72	84%
	KO	0.86	0.74	0.79	

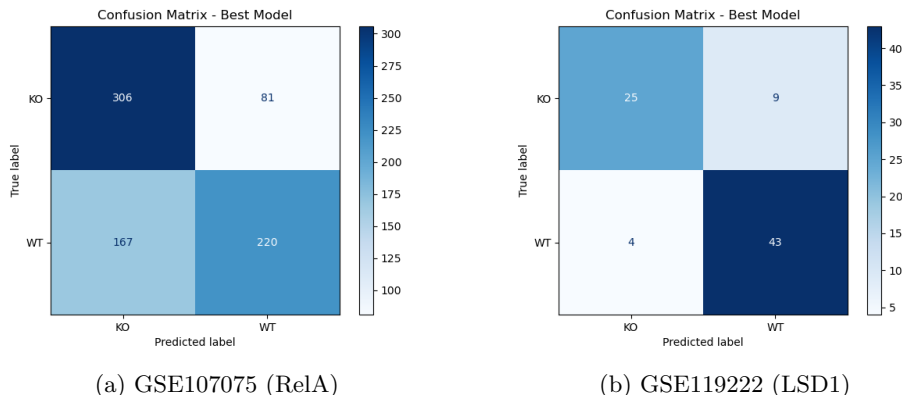


Figure 5: WT vs KO Peak Prediction. Training is done using chromosomes 1 to 19, except chromosomes 6 and 7 and Testing using chromosomes 6 and 7.

Figure 6 shows the training (blue) and test (orange) accuracy curves across all epochs. Both curves gradually increased and stabilized, with the test accuracy. The model achieving the highest test accuracy was saved as the final model for downstream saliency and motif analyses. The small gap between training and test accuracy indicates that the model generalized well without substantial overfitting.

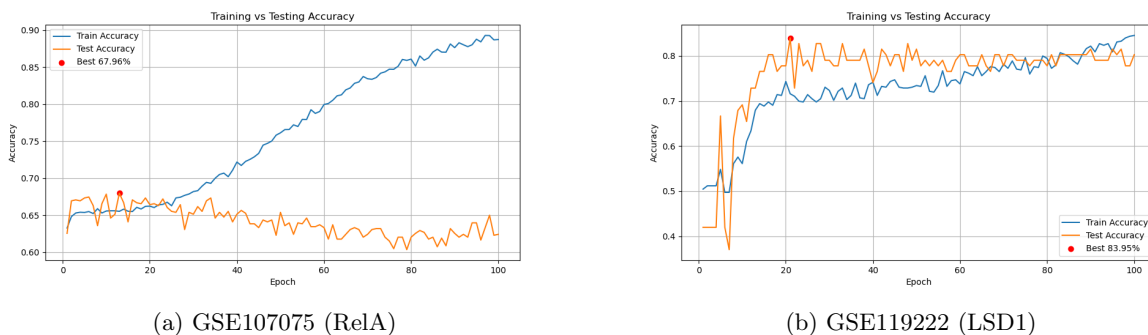


Figure 6: Training and test accuracy curves per epoch for two datasets. For each dataset, the CNN-attention models training (blue) and test (orange) accuracy are shown. Red dots indicate epochs with the highest test accuracy.

## 4.2 Saliency-Based Identification of Regulatory Sequence Features

To interpret the features driving CNN attention predictions, we computed gradient-based saliency maps for each sequence in the test set (Chr6 and Chr7). The three positions with the highest saliency scores are selected per sequence, and 20-bp k-mers centered on these positions are extracted as candidate regulatory elements (Figure 7). Saliency analysis revealed that model predictions are influenced by specific sequence motifs rather than distributed noise across the input, indicating that the model captured biologically meaningful patterns.

Sample saliency maps illustrating nucleotide-level importance for model predictions are shown in Figure 7. For each dataset, two sequences from the held-out test set are selected to visualize the positional contribution of nucleotides to the classification decision. Regions with high saliency values indicate sequence positions that most strongly influenced the CNN-attention model.

## 4.3 Motif Discovery and Enrichment Analysis

In this step, we flattened the top k-mers extracted from high-saliency positions into a single table and clustered using hierarchical agglomerative clustering based on cosine distance to group similar sequence

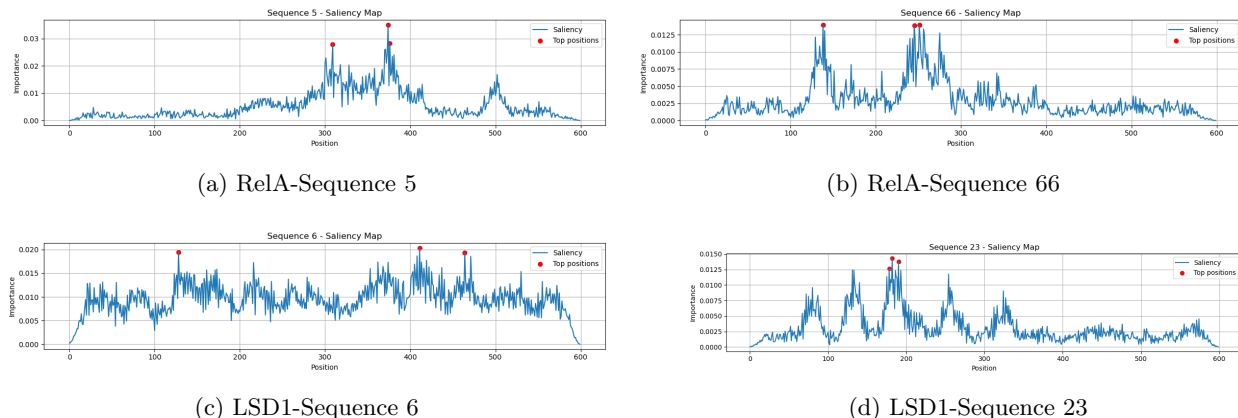


Figure 7: Sample saliency maps illustrating nucleotide-level importance across test genomic sequences of RelA and LSD1 Dataset. Peaks in saliency highlight regions contributing most strongly to model predictions.

patterns. For each cluster, we generated a consensus motif by selecting the most frequent nucleotide at each position and then de novo motif discovery was performed using MEME. Further, MEME generated motifs are compared against known transcription factor binding sites using TOMTOM. Clusters with fewer than 10 k-mers are not analyzed with MEME/TOMTOM due to insufficient sequence numbers for reliable motif inference. A list of consensus motifs are given in Table 5 for RelA and Table 6 for LSD1. We considered 10 clusters for RelA. As the number of test sequences for LSD1 was smaller, we considered 6 clusters for LSD1.

Top transcription factor matches and their respective families are annotated based on TOMTOM results are shown in Table 7 and Table 8. This analysis revealed that many high-saliency clusters correspond to biologically relevant motifs, including members of the bZIP family (FOS, JUNB, BATF), bHLH (ASCL1, TCF4) and C2H2 zinc finger factors (KLF4, KLF5), providing mechanistic insight into the regulatory grammar learned by the model. Table 7 and Table 8 summarizes representative clusters, including consensus motifs, motif logos, top transcription factor matches, and their families of RelA dataset. This cluster-wise approach allowed identification of both common and condition-specific motifs, reflecting differential regulatory patterns between WT and KO sequences.

Clusters containing at least 10 k-mers are considered for motif analysis. Among these, the cluster with the largest number of k-mers are treated as the primary discriminative transcription factor (TF) between WT and KO, while the remaining clusters are considered secondary discriminative TFs. Cluster 4 for RelA and Cluster 1 for LSD1 contained the most k-mers and are treated as primary discriminative clusters, with the remaining clusters considered secondary. It can be seen from the tables, bZIP family (FOS, JUN, ATF3) acts as the primary discriminative TF for RelA, whereas bHLH (ASCL1, TCH4) family for LSD1. All TOMTOM results are added in Supplementary Folder S4.

Table 5: Consensus motifs derived from clustered high-saliency k-mers for RelA Dataset. Each cluster groups k-mers with similar sequences, and the count indicates the number of k-mers in that cluster.

Cluster ID	Consensus Sequence	Count
0	CCTGGCTGCTTCTTCTGCC	221
1	GCGGATTGCTTGAGAAAATT	271
2	TTTCTGTTTCTTTTGTTTT	236
3	TGAAACCAGGAAACTAGGCT	260
4	GGGGGTCTGGGACAGAGGCG	336
5	TTCCAGGCCGTGGTGGGCG	156
6	AGCCTTATTTCTGCCCAAAG	99
7	AAAAAAGAGAAAAAGAAA	350
8	GATTCTCTGATCATGTTGGG	162
9	CCCCCCTCCGCCCCCGC	231

Table 6: Consensus motifs obtained from clustering saliency-derived k-mers for LSD1 binding sequences. Each cluster groups k-mers with similar sequences, and the count indicates the number of k-mers in that cluster.





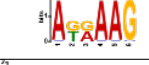

Cluster ID	Consensus Sequence	Count
0	GCCCGGACCGGCTGCCGGGC	40
1	CCGCCCCCCCCCCCCCCCC	111
2	GGCGCCCCGCCGCACAGCG	15
3	AAAGTCTGTCGTAGATTCA	3
4	TCCGGAGCAACAGGGAGAAG	11
5	GGGAGGCAGGCGGGCCCGCA	63

Table 7: Summary of cluster-wise MEME motifs derived from high-saliency k-mers and Matched TFs from TOMTOM of RelA Dataset.

Cluster ID	MEME Motif	Motif Logo	Top TF match(s)	Family
0	SYCABTGCCTSC		EHF, ELF3, ELF1 MAFK, NFE2	ETS
1	CCACGCGCATCC		KLF6, SP8, KLF11, SP9, SP3	C2H2 zinc finger
1	KCCAYGWCTCAG		ATF1, FOS, FOSL2, BACH2	bZIP
2	GSBTGWSWGMSH		MAF, MAFA, MAFK	bZIP
4	MTGASWCA		MAFG, JDP2, BNC2, MAFK JUNB, JUND, NFE2	bZIP
4	TGACDTCMTSCR		ATF3, FOS::JUN, FOSL2::JUNB, ETV1, ELK4, ETS1, FOS, JUN	bZIP
5	TCAGGTTATA		Six4, SIX1, SIX2	bZIP
6	STTTTRGTTK		IRF8, IRF5, IRF4, RUNX1	Tryptophan cluster, Runt
7	GRRACAGWCAT		NFE2, Stat2, FOS::JUND	bZIP
8	ASTRAGTCAS		BNC2, Atf3, BATF::JUN	bZIP
9	RACTCATCTGA		NFE2, Jun, FOS	bHLH, bZIP

These results indicate that WTKO-CNN not only provides accurate predictions of condition-specific accessibility but also enables mechanistic insights by linking sequence patterns to potential regulatory elements affected by gene knockout. By combining predictive performance with interpretability, the framework offers a powerful approach for dissecting the sequence basis of differential chromatin landscapes.

Table 8: Summary of cluster-wise MEME motifs derived from high-saliency k-mers and Matched TFs from TOMTOM of LSD1 Dataset.

Cluster ID	MEME Motif	Motif Logo	Top TF match(s)	Family
0	CCCTGCT		ZIC3, ZIC1, ZIC2	C2H2 zinc finger
1	WGNSADCCTGCT		TCF4, Zic3, ASCL1, TCF12	bHLH
1	AGRBCKGSSKGC		KLF7, SP2, KLF1	C2H2 zinc finger
2	CACGTG		MAX, Mlxip, MNT	bHLH-ZIP
4	AKRAAG		Elf5, ELF1, ETV1, EHF, ETS1	ETS
4	CMKRRGCAGCWG		Ptf1A, Neurod2, Twist2, Fli1	Tal-related bHLH

#### 4.4 Discriminative Motifs Identified by CNN Filter

Saliency analysis identifies the most important positions within individual sequences, while CNN filter k-mers reveal global motifs learned across the dataset. Together, these analyses provide a comprehensive view of both sequence-specific and shared regulatory features. To further characterize sequence features learned by the model, we analyzed activations of the first convolutional layer (64 filters, kernel size 10) for 5 runs. For each filter, we identified the top activations across all sequences and extracted the corresponding k-mers from the input DNA.

These k-mers are aggregated to generate a consensus motif per filter, representing the sequence pattern that most strongly activates that filter. Then Significant motifs are then matched to known transcription factors using Tomtom against the JASPAR 2022 vertebrate database (p-value < 0.05).

Table 9 and 10 summarizes the top discriminative sequence motifs identified from WT vs KO RelA and LSD1 peaks using saliency-derived k-mers followed by motif clustering and MEME analysis. The identified motifs correspond to transcription factor families known to play roles in transcriptional regulation and chromatin accessibility. Notably, For RelA dataset, motifs matching the AP-1 family (FOS, JUN, BATF) are detected, consistent with the known regulatory interactions between AP-1 and NF-B signaling pathways. In addition, GC-rich motifs associated with SP family transcription factors (SP1, SP2, SP4) are identified, suggesting potential involvement of GC-binding regulatory elements in the differential binding landscape. These results indicate that CNN Filter-driven motif discovery can capture biologically meaningful transcription factor signatures that may contribute to the observed differences between WT and KO conditions. For LSD1, motifs identified from MEME for these clusters correspond to sequences such as CCSCGCGCCC, and TOMTOM analysis matched these motifs to transcription factors including KLF16, SP1, SP2, HES1, TCF4, and ZIC1.

Table 9: Discriminative motifs identified from WT versus KO RelA peaks. Motifs are shown with representative sequence logos, consensus motifs, and matched transcription factor families.






Dataset	Motif Logo	MEME MOTIF	Matched TFs	Family
RelA		GWSWCTCA	FOS, ATF3, BNC2	bZIP
RelA		TGTGKCAC	BATF::JUN, FOS::JUN, FOSB::JUNB	bZIP
RelA		CCCKMCWC	SP1,SP2, SP4	C2H2

Table 10: Discriminative motifs identified from WT versus KO LSD1 peaks. Motifs are shown with representative sequence logos, consensus motifs, and matched transcription factor families.

Dataset	Motif Logo	MEME MOTIF	Matched TFs	Family
LSD1		CCSCGCGCCC	KLF16, SP1, SP2, KLF1, KLF12	C2H2
LSD1		CCSCGCGCCC	HES1, TCF4, ZIC1	bHLH

## 5 Validation

To validate the regulatory motifs identified by our WTKO-CNN model, we performed motif enrichment analysis using HOMER on high-saliency peaks from WT and KO test datasets (held out chromosomes).

### 5.1 HOMER Motif Enrichment Of RelA Chr6 and Chr7 WT and KO Peaks Validates WTKO-CNN Predictions

RelA WT and KO test sequences derived from Chr6 and Chr7 are used for motif enrichment analysis. The sequences are analyzed using the HOMER motif discovery tool [22] (findMotifsGenome.pl) to identify significantly enriched motifs at peak regions. HOMER performs enrichment analysis by comparing the input sequences against background genomic regions and identifying overrepresented motifs that may correspond to regulatory elements. Table 11 summarizes the most enriched motifs, including the consensus sequence,

Table 11: HOMER motif enrichment analysis of RelA Chr6 and Chr7 peaks for WT and KO datasets. Top transcription factor motifs show differential prevalence between conditions.

Motif Name	Consensus	% Target (WT)	% Target (KO)	p-value (WT)	p-value (KO)
FOS (bZIP)	NDATGASTCAYN	36.95%	59.80%	$1 \times 10^{-87}$	$1 \times 10^{-268}$
ATF3 (bZIP)	DATGASTCATHN	36.95%	60.46%	$1 \times 10^{-79}$	$1 \times 10^{-254}$
BATF (bZIP)	DATGASTCAT	37.47%	60.46%	$1 \times 10^{-80}$	$1 \times 10^{-252}$
JunB (bZIP)	RATGASTCAT	35.14%	56.86%	$1 \times 10^{-81}$	$1 \times 10^{-253}$
Fosl2 (bZIP)	NATGASTCABNN	26.87%	44.12%	$1 \times 10^{-69}$	$1 \times 10^{-218}$
KLF5 (C2H2 ZF)	DGGGYGKGGC	20.67 %	7.03%	$1 \times 10^{-7}$	$1 \times 10^{-4}$
MafK (bZIP)	GCTGASTCAGCA	6.46%	12.58%	$1 \times 10^{-4}$	$1 \times 10^{-27}$

percentage of target peaks containing the motif, and associated p-values. Notably, several bZIP family TFs, such as FOS, ATF3, BATF, JunB, and Fosl2, showed higher enrichment in KO peaks compared to WT, both in terms of the fraction of peaks containing the motif and statistical significance. In contrast, the C2H2 zinc finger TF KLF5 exhibited stronger enrichment in WT peaks, with a reduction in KO, suggesting differential regulation. These results highlight that loss of RelA alters the chromatin landscape, preferentially affecting motifs recognized by bZIP TFs, and provides a basis for linking motif changes to transcriptional reprogramming in KO cells. Figure 8 shows the percentage of target sequences containing each motif in WT and KO conditions. A full list of all enriched motifs and associated statistics is provided in Supplementary File S2 and S3. These results provide independent validation of the proposed model’s predictions and demonstrate that the identified motifs reflect genuine transcription factor binding preferences. While HOMER identifies statistically enriched motifs in target sequences, it often generates long lists of motifs, including many redundant or non-discriminative hits. In contrast, our WTKO-CNN framework directly learns sequence features that drive classification between WT and KO conditions. By combining saliency mapping and clustering of top k-mers, we focus on biologically relevant motifs, capturing context-dependent and combinatorial patterns that HOMER alone may overlook.

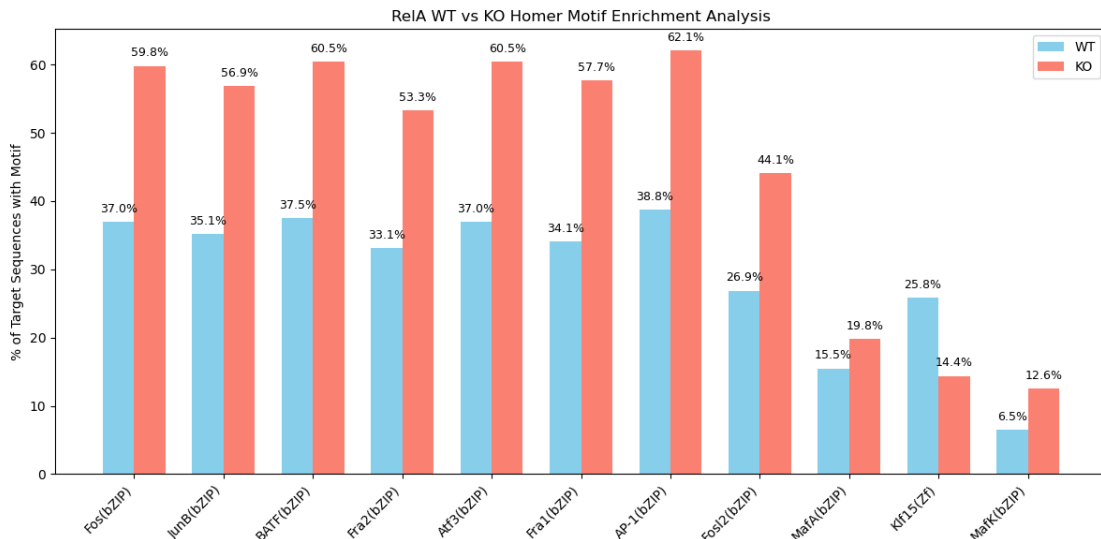


Figure 8: RelA WT vs KO Chr6 and Chr7 Homer Motif Enrichment Analysis.

## 5.2 HOMER Motif Enrichment Of LSD1 Chr6 and Chr7 WT and KO Peaks Validates WTKO-CNN Predictions

To investigate transcription factor (TF) binding changes upon LSD1 deletion, We analyzed both LSD1 WT and KO samples to assess changes in motif enrichment. Homer motif analysis revealed on whole LSD1 WT and KO that, bHLH transcription factor motifs are significantly enriched at peak regions, consistent with active binding of factors such as HEB, E2A, Ascl1, and Ptf1a (Supplementary File 2). In contrast, in LSD1 knockout (KO) cells, bHLH motifs are largely absent, indicating a loss of accessibility at these sites. This suggests that bHLH factor binding is required for LSD1 chromatin states, and its deletion disrupts the recruitment of these transcriptional regulators. For LSD1 chromosomes 6 and 7, shared motifs highlighted conserved regulatory elements, with ETS family motifs, including ETS1, ELF5 (Figure 9). bHLH family motifs, such as NeuroG2, Twist2, and BHLHA15, are also present in both conditions. Quantification of target sequences containing each motif revealed differences in relative enrichment; for example, NeuroG2 and BHLHA15 showed higher prevalence in WT, suggesting potential compensatory regulatory activity or altered chromatin accessibility. These trends are visualized using bar plots showing the percentage of target sequences with each motif, providing a clear view of transcription factor occupancy shifts associated with LSD1 loss on chromosomes 6 and 7.

Table 12: HOMER motif enrichment analysis of LSD1 Chr6 and Chr7 peaks for WT and KO datasets. Top transcription factor motifs show differential prevalence between conditions.

Motif Name	Consensus	% Target (WT)	% Target (KO)	p-value (WT)	p-value (KO)
ETS1 (ETS)	ACAGGAAGTG	44.68%	19.32%	$1 \times 10^{-7}$	$1 \times 10^{-1}$
ELF5(ETS)	ACVAGGAAGT	29.79%	12.50%	$1 \times 10^{-5}$	$1 \times 10^{-1}$
Fli1(ETS)	NRYTCCCGH	36.17%	19.32%	$1 \times 10^{-4}$	$1 \times 10^{-1}$
ERG(ETS)	ACAGGAAGTG	44.68%	22.73%	$1 \times 10^{-4}$	$1 \times 10^{-1}$
Twist2(bHLH)	MCAGCTGBYH	51.06%	9.09%	$1 \times 10^{-4}$	$1 \times 10^{-0}$
Max(bHLH)	RCCACGTGGYYN	25.5%	4.55%	$1 \times 10^{-3}$	$1 \times 10^{-0}$
Ptf1a(bHLH)	ACAGCTGTTN	63.83%	22.73 %	$1 \times 10^{-3}$	$1 \times 10^{-0}$

These results provide independent validation of the proposed model’s predictions and demonstrate that the identified motifs reflect genuine transcription factor binding preferences. While HOMER identifies statistically enriched motifs in target sequences, it often generates long lists of motifs, including many redundant

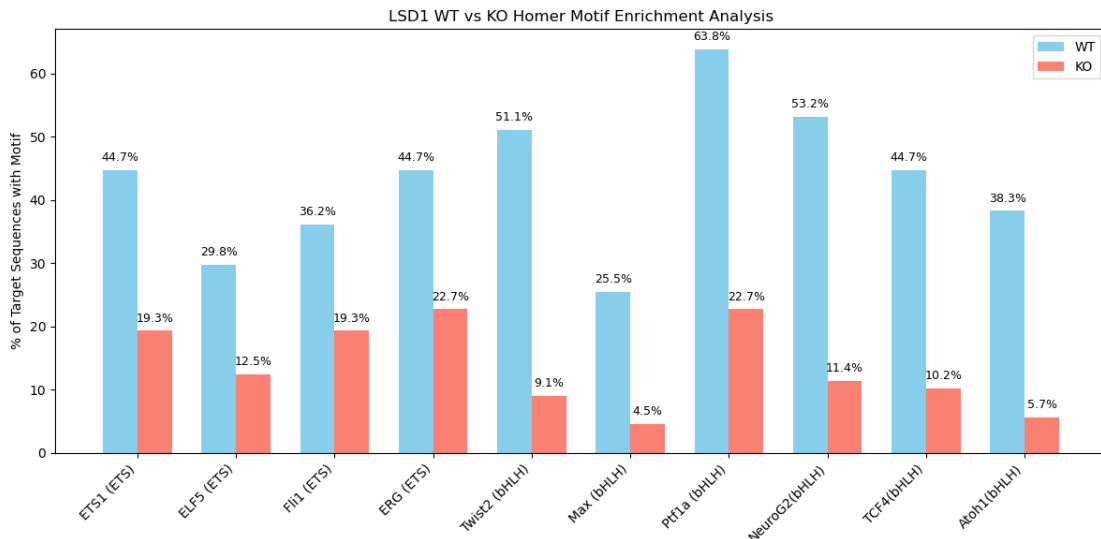


Figure 9: LSD1 WT vs KO Chr6 and Chr7 Homer Motif Enrichment Analysis.

or non-discriminative hits. In contrast, our WTKO-CNN framework directly learns sequence features that drive classification between WT and KO conditions. By combining saliency mapping and clustering of top k-mers, we focus on biologically relevant motifs, capturing context-dependent and combinatorial patterns that HOMER alone may overlook.

For LSD1, Homer analysis of chromosomes 6 and 7 test sequences revealed that ETS motifs are more abundant in WT sequences. However, the CNN-attention model identified bHLH motifs as the primary discriminative TF. This indicates that, although ETS motifs are enriched in WT, the predictive power of the model for distinguishing WT from KO sequences relies predominantly on bHLH motifs, highlighting their functional importance in driving WT-specific chromatin accessibility.

## 6 Comparison with Other Algorithms

We examined several sequence classification models: CNN with 4 Layers, a hybrid CNN+LSTM model and Vanilla Transformer model to assess how well various deep learning architectures predicted chromatin accessibility patterns between WT and KO situations. The proposed WTKO-CNN using sequence input performed the best out of all the models, demonstrating its great ability to extract and use local sequence characteristics that are essential for differentiating between WT and KO peaks.

We implemented a deep learning architecture consisting of four stacked convolutional neural network (CNN) layers. This model is designed to progressively extract hierarchical features from DNA sequences, where early layers capture simple local motifs and deeper layers learn more complex and abstract sequence patterns. By stacking multiple convolutional layers, the network is able to effectively model spatial dependencies within short genomic regions that are often biologically relevant.

In the CNN+LSTM model, a Long Short-Term Memory (LSTM) network is applied after the CNN layers to capture long-range dependencies and sequential patterns in the data. This hybrid architecture enables the model to learn relationships between nucleotides that may be distant in the sequence, but biologically significant. The LSTM layer retains important contextual information throughout the sequence, complementing the local feature extraction performed by the CNN. Finally, the output of the LSTM is passed through a fully connected layer for classification, allowing the model to predict whether a given DNA sequence belongs to the WT or KO category. This combined approach leverages the strengths of CNNs in capturing local motifs and LSTMs in modeling global sequence dependencies, making it particularly effective for DNA sequence classification tasks where both short- and long-range interactions are important.

We also implemented a Transformer-based model to predict chromatin accessibility states for WT and

KO sequences. Unlike BERT-based approaches that rely on large-scale pretraining, our vanilla Transformer is trained from scratch on the target dataset. The model begins with an embedding layer that converts DNA sequences into dense numerical representations. These embeddings are then passed through multiple Transformer encoder layers, which use self-attention mechanisms to capture long-range dependencies and complex interactions across the sequence. This allows the model to learn global contextual relationships without relying on recurrence or convolution. The final representation is fed into a classification head to predict chromatin accessibility states.

The CNN+Transformer model achieved consistent performance across both datasets. On GSE107075 (RelA), it obtained WT scores of 0.70 precision, 0.40 recall, and 0.51 F1-score, while KO reached 0.58 precision, 0.82 recall, and 0.68 F1-score, resulting in an overall accuracy of 62%. On GSE119222 (LSD1), the model showed similar stability with WT scores of 0.55 precision, 0.71 recall, and 0.62 F1-score, and KO scores of 0.73 precision, 0.57 recall, and 0.64 F1-score, achieving an overall accuracy of 63%.

The Table 13 shows that the proposed WTKO-CNN model consistently outperforms the other evaluated architectures, including CNN, CNN+LSTM, CNN+Transformer and the vanilla Transformer, across both datasets (GSE107075 and GSE119222). It achieves the highest overall accuracy, reaching up to 84% on GSE119222, demonstrating a substantial improvement over competing methods. In addition to improved accuracy, WTKO-CNN shows stronger and more balanced performance in precision, recall, and F1-score for both WT and KO classes, indicating better discrimination capability and reduced classification bias (Figure 10).

This improvement can be attributed to the models tailored architecture, which is specifically designed to capture class-relevant patterns distinguishing WT and KO sequences. Unlike CNN-only models that primarily focus on local motif detection or CNN+LSTM models that may struggle with long-range dependency optimization, WTKO-CNN effectively integrates feature learning in a way that enhances both local and global sequence representation. Compared to the Transformer model trained from scratch, WTKO-CNN demonstrates better generalization on limited genomic datasets, likely due to its more efficient inductive bias for sequence-based biological signals. Overall, these results highlight the robustness and effectiveness of WTKO-CNN for chromatin accessibility and DNA sequence classification tasks.

Table 13: Performance comparison of different models across datasets.

Algorithm	Dataset	Class	Precision	Recall	F1-score	Accuracy
CNN 4 layers	GSE107075 (RelA)	WT	0.69	0.49	0.57	64%
		KO	0.61	0.79	0.68	
	GSE119222 (LSD1)	WT	0.42	0.59	0.49	65%
		KO	0.65	0.89	0.75	
CNN+LSTM	GSE119222 (RelA)	WT	0.65	0.54	0.59	63%
		KO	0.61	0.71	0.66	
	GSE107075 (LSD1)	WT	0.59	0.68	0.63	54%
		KO	0.44	0.35	0.39	
Vanilla Transformer	GSE107075 (RelA)	WT	0.58	0.77	0.66	60%
		KO	0.65	0.44	0.53	
	GSE119222 (LSD1)	WT	0.59	0.75	0.66	62%
		KO	0.68	0.50	0.51	
CNN+Transformer	GSE107075 (RelA)	WT	0.70	0.40	0.51	62%
		KO	0.58	0.82	0.68	
	GSE119222 (LSD1)	WT	0.55	0.71	0.62	63%
		KO	0.73	0.57	0.64	
<b>WTKO-CNN</b>	GSE107075 (RelA)	WT	0.73	0.57	0.64	<b>68%</b>
		KO	0.65	0.79	0.71	
	GSE119222 (LSD1)	WT	0.83	0.87	0.72	<b>84%</b>
		KO	0.86	0.74	0.79	

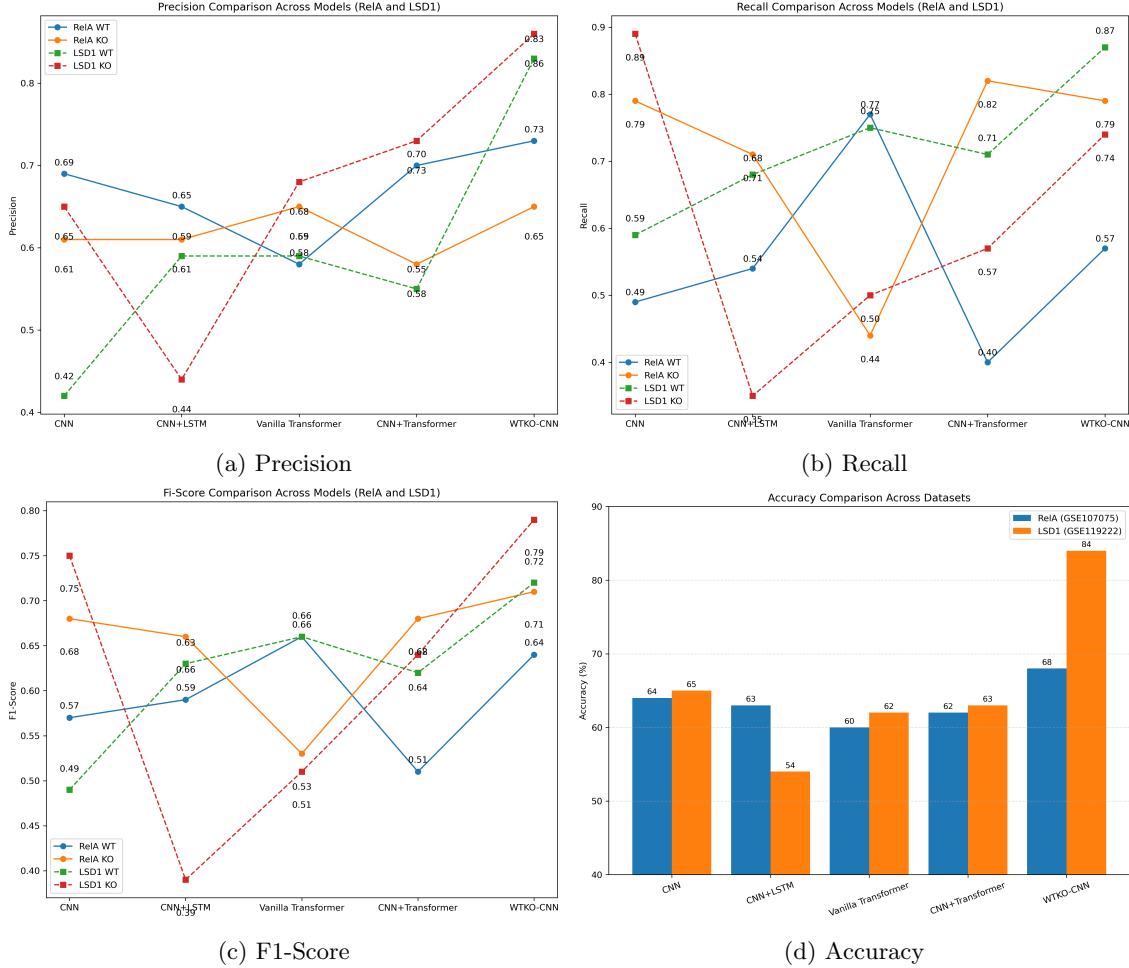


Figure 10: Comparative evaluation of model performance on RelA and LSD1 datasets. The subfigures illustrate (a) Precision, (b) Recall, (c) F1-score, and (d) Accuracy. The proposed WTKO-CNN model consistently outperforms baseline approaches, demonstrating improved robustness and balanced classification across WT and KO classes.

## 7 Conclusion

Transcriptional regulation mechanisms requires an understanding of the regulatory sequence characteristics that influence condition-specific chromatin accessibility. Here, we created a WTKO-CNN, a one-dimensional convolutional neural network with an attention mechanism, to categorise genomic sequences as either KO-specific or WT. While traditional tools such as HOMER successfully identified primary overrepresented motifs (e.g., RelA and LSD1), our CNN-attention framework provided a distinct advantage by highlighting regulatory features. Unlike frequency-based enrichment approaches, saliency maps pinpointed nucleotide clusters that are functionally critical for the models classification performance. This enabled the discovery of non-canonical motifs and structural features, potentially representing secondary recruitment mechanisms or DNA shape constraints that govern differential accessibility in the KO condition.

## Supplementary Information

Supplementary data associated with this article are available online.

Supplementary File S1: S1 contains experimentally generated WT and KO peaks of RelA and LSD1.

Supplementary Files S2 and S3: S2 contains Homer Motif Enrichment Results of Test Sequences, Chromo-

some 6 and 7 of RelA and LSD1 and S3 contains the Homer Motif Enrichment Results of all Peaks of RelA and LSD1.

Supplementary Folder S4: All TOMTOM results of each cluster MEME motifs.

## References

- [1] Timothy L Bailey et al. “MEME SUITE: tools for motif discovery and searching”. In: *Nucleic acids research* 37.suppl.2 (2009), W202–W208.
- [2] Mohamed A El-Brolosy et al. “Genetic compensation triggered by mutant mRNA degradation”. In: *Nature* 568.7751 (2019), pp. 193–197.
- [3] Rémi-Xavier Coux, Nick DL Owens, and Pablo Navarro. “Chromatin accessibility and transcription factor binding through the perspective of mitosis”. In: *Transcription* 11.5 (2020), pp. 236–240.
- [4] Philipp Godbersen, Daniel Schanz, and Andreas Schröder. “Peak-CNN: improved particle image localization using single-stage CNNs”. In: *Experiments in Fluids* 65.10 (2024), p. 153.
- [5] Hemalatha Gunasekaran et al. “Analysis of DNA sequence classification using CNN and hybrid models”. In: *Computational and Mathematical Methods in Medicine* 2021.1 (2021), p. 1835056.
- [6] Katerina Hatzi et al. “Histone demethylase LSD1 is required for germinal center formation and BCL6-driven lymphomagenesis”. In: *Nature immunology* 20.1 (2019), pp. 86–96.
- [7] Alexander Kensert et al. “Convolutional neural network for automated peak detection in reversed-phase liquid chromatography”. In: *Journal of Chromatography A* 1672 (2022), p. 463005.
- [8] Peter K Koo and Matt Ploenzke. “Improving representations of genomic sequence motifs in convolutional networks with exponential activations”. In: *Nature machine intelligence* 3.3 (2021), pp. 258–266.
- [9] Jack Lanchantin et al. “Deep motif dashboard: visualizing and understanding genomic sequences using deep neural networks”. In: *Pacific symposium on biocomputing 2017*. World Scientific. 2017, pp. 254–265.
- [10] Heyi Li et al. “Beyond saliency: understanding convolutional neural networks from saliency prediction on layer-wise relevance propagation”. In: *Image and Vision Computing* 83 (2019), pp. 70–86.
- [11] Junbing Li et al. “Deep-LIFT: Deep label-specific feature learning for image annotation”. In: *IEEE transactions on Cybernetics* 52.8 (2021), pp. 7732–7741.
- [12] Luca Mariani et al. “MEDEA: analysis of transcription factor binding motifs in accessible chromatin”. In: *Genome Research* 30.5 (2020), pp. 736–748.
- [13] Gherman Novakovsky et al. “ExplaiNN: interpretable and transparent neural networks for genomics”. In: *Genome Biology* 24.1 (2023), p. 154.
- [14] Dongpin Oh et al. “CNN-Peaks: ChIP-Seq peak detection pipeline using convolutional neural networks that imitate human visual inspection”. In: *Scientific reports* 10.1 (2020), p. 7933.
- [15] Amine M Remita and Abdoulaye Baniré Diallo. “Statistical linear models in virus genomic alignment-free classification: application to hepatitis C viruses”. In: *2019 IEEE International Conference on Bioinformatics and Biomedicine (BIBM)*. IEEE. 2019, pp. 474–481.
- [16] Jake J Reske, Mike R Wilson, and Ronald L Chandler. “ATAC-seq normalization method can significantly affect differential accessibility analysis and interpretation”. In: *Epigenetics & chromatin* 13 (2020), pp. 1–17.
- [17] François Spitz and Eileen EM Furlong. “Transcription factors: from enhancer binding to developmental control”. In: *Nature reviews genetics* 13.9 (2012), pp. 613–626.
- [18] Abdulkadir Tasdelen and Baha Sen. “A hybrid CNN-LSTM model for pre-miRNA classification”. In: *Scientific reports* 11.1 (2021), p. 14125.

- [19] Meng Wang et al. “DeFine: deep convolutional neural networks accurately quantify intensities of transcription factor-DNA binding and facilitate evaluation of functional non-coding variants”. In: *Nucleic acids research* 46.11 (2018), e69–e69.
- [20] Y Xu et al. “TRAFICA: Improving Transcription Factor Binding Affinity Prediction using Deep Language Model on ATAC-seq Data”. In: (2023).
- [21] Jinyu Yang et al. “Prediction of regulatory motifs from human Chip-sequencing data using a deep learning framework”. In: *Nucleic acids research* 47.15 (2019), pp. 7809–7824.
- [22] Fan Zhang and Jake Y Chen. “HOMER: a human organ-specific molecular electronic repository”. In: *BMC bioinformatics* 12.Suppl 10 (2011), S4.
- [23] Shuangquan Zhang et al. “Assessing deep learning methods in cis-regulatory motif finding based on genomic sequencing data”. In: *Briefings in Bioinformatics* 23.1 (2022), bbab374.
- [24] Xiangxie Zhang et al. “Comparing machine learning algorithms with or without feature extraction for DNA classification”. In: *arXiv preprint arXiv:2011.00485* (2020).
- [25] Yongqing Zhang et al. “CAE-CNN: Predicting transcription factor binding site with convolutional autoencoder and convolutional neural network”. In: *Expert Systems with Applications* 183 (2021), p. 115404.
- [26] Jian Zhou and Olga G Troyanskaya. “Predicting effects of noncoding variants with deep learning-based sequence model”. In: *Nature methods* 12.10 (2015), pp. 931–934.